Time-resolved imaging of model astrophysical jets

Theodoros Smponias[1]

PO box 5, PO 2, Ioannina, Greece

Abstract

An approximate, time-delayed imaging algorithm is implemented, within existing line-of-sight code. The resulting program acts on hydrocode output data, producing synthetic images, depicting what a model relativistic astrophysical jet looks like to a stationary observer. As part of a suite of imaging and simulation tools, the software is able to visualize a variety of dynamical astrophysical phenomena. A number of tests are performed, in order to confirm code integrity, and to present features of the software. The above demonstrate the potential of the computer program to help interpret astrophysical jet observations.

Keywords:

ISM: jets and outflows, stars: winds-outflows, stars: flare, radiation

mechanisms: general, methods: numerical

2010 MSC: 85-08

1. Introduction

SOS 290319 briefly xplain the reasoning behind each test (clight, ts, etc) right where those tests are first presented.

SOS 290319 Add the tests on SR imaging (steadsy-state ones) vs Kraus etc from the lit., . Move all tests to Appendix. only keep APP in main text.

1. sphere. st state. static and moving sphere.

2. rod, as aportion of a cylindrical jet. (should be implemented already)

---

*Corresponding author

Email address:* `t.smponias@hushmail.com` (Theodoros Smponias)

3. A sphere emitting isotropically, transformed to the obs frame. based on hughes 91

4. A st. state hj88 type jet, transformed to the obs frame. based on cawthorne in hughes 91.

5. A, optically thin SYNCHROTRON st. state hj88 type jet, transformed to the obs frame. also based on cawthorne 91, a bit later on (simple synchr. jet dependent on sin theta dash: S(nu, theta)=Snu(dash)Dtothe(3+a), or 2+a for simple jets (replies to ref2 comment)

Comment: a tangled B field also contributes to the synchrotron emission being isotropic. see if this is the case for thermal or radio as well.

some good refs from cawthorne 91: BBRees84 and RL79 chapter 4. SOS re-examine those SOS.

SOS briefly explain the reasoning behind each test, such as clight, ts, etc.

SOS HERE describe focuing of the beams and add a relevant figure. SOS 040419

compare focused results to the kraus et al results. SOS

move sall tests to the appendix only keep basics in main text.

INTRO make bigger, adding in more detail where exactly these simulations are needed. SOS

ROD TEST: kraus et al pre-applies length contraction then runs their sp. relat. ray tracing model. We do not pre-apply length contraction, say that and take into account whemn comparing.

040419 we may improve on the steady state tests by incorporating elements from computer graphics, such as parametric moving object representation. Also, we do not adopt diffraction,e tc, only a straight line of sight. XPLAIN that!

Imaging a relativistically-moving macroscopical object, opens a window to a rather unexpected and even strange world of peculiarities. The basic mandates of Special Relativity, regarding length contraction and time dilation, constitute a mere beginning, in the quest for comprehension of the actual appearance of a fast-moving object [1, 2, 3, 4, 5]. Looking at the latter, travelling in front of the eye or the telescope, an observer shall *see* the object view affected by a number

of relativistic distortions [6, 7, 8].

In order to simulate the observation of a relativistic astrophysical jet (for example [9]), a model requires a stationary observer, and a fast-moving gaseous mass, comprising both the jet and some of its surrounding matter. The transformation of electromagnetic emissions, from the jet's frame of reference to the Earth frame, requires performing the Lorentz/Poincaré transform[10, 11, 12, 6].

Applying the latter transform for imaging purposes, aims to recons truct what the observer will actually see, as opposed to what is measured. Relevant to this point, [13] argues about the important difference between vision and measurement in Special Relativity, presenting that difference in a geometrical manner.

Radiation emitted from a jet is therefore subject to relativistic effects [14, 11], including time dilation, relativistic aberration and frequency shift, leading collectively to what is known as Doppler boosting and beaming [12, 6, 15]. Aberration causes the fast-moving object to actually appear *rotated* to a stationary observer [2, 3, 16, 6], a phenomenon sometimes called the Terell-Penrose rotation.

[17, 18] provide an early computerized attempt to reconstruct a relativistic image, through the eyes of an observer crossing a scene at high velocity. [19] demonstrates the importance of the relativistic transform of brightness and color. When imaging a jet, these correspond to Doppler boosting and frequency shift, respectively. [19] discusses an object that moves at uniform speed across the field of view, but is visually large enough for the angle between velocity and line of sight to vary along the object. Applying the Lorentz transform changes brightness and color in a separate manner, for each point of the observed object. [6] improves on such calculations, providing various methods for relativistic visualization, in both Special and General relativistic frameworks.

[20] calculate the visual appearance of wireframe relativistic objects, by mathematically inverting the course of light, from an image point to the emission event. They provide expressions that directly describe how a series of objects would look like, when moving at high speed, in front of a stationary observer. The efficiency of their method is then compared to the increased detail of a

3

related ray-tracing project [21]. [15] image scenes with a fast observer traveling through their artificial environment. They also relate their simulations to actual imaging experiments, using the femto-photography technique [22]. Furthermore, they introduce a number of additional details into their models, such as camera distortions from traveling at very high speed. [23] present a framework, where the subject of relativistic imaging is explored, in a scientifically correct and accessible manner.

Even though ray-tracing methods provide excellent quality of relativistic images, they still lack in terms of efficiency, compared to such techniques as polygon rendering [8]. In the current paper, a hybrid relativistic imaging method is presented, whereby time-resolved hydrocode data are being crossed by lines of sight (LOS), parallel to each other. Most relativistic effects are directly incorporated, the rest being represented approximately. Some accuracy is thus traded for increased efficiency, allowing for near-real time relativistic imaging of evolving model jets, with modest computing resources.

SOS 290319 HERE ADD some intro stuff on the application (microquasar, etc.) Also the neutrino stuff. DACE PSO perhaps etc. SOS

In the remaining of this paper, the methodology used in the imaging process, in order to draw the synthetic image, is presented first (Section 3). We then proceed to briefly describe the new program itself, called RLOS (Relativistic Line Of Sight) (Section 6). Code tests are then provided, whereby imaging is executed repeatedly, with different settings, based on just a few underlying hydrocode runs. Through artificially altering certain parameters in post-processing, imaging code behaviour is explored, and results are discussed (Section 7). Finally, in Section 8 useful conclusions are drawn from the current work and possible future applications are proposed.

4

2. Background and goals

2.1. Aims of the sims

Relativistic jets constitute a physical laboratory of extreme conditions in the Universe. They allow us to study a vsariety of phenomena where many physical theories may be put to the test. Nevertheless, their distance means that images at various bands are rather faint and also their spectra are not as detailed as those of nearer objects. Consequently, we may resort to numerical experiments. We setup a model of the astro-system, select the initial and boundary conditions and then run the model. The model produces synthetic iamges and spectra. If these match the observed ones, then we assume that the model inputs match the conditions of the real system. If no match is achieves we change the model inputs until a reasonable match is obtained.

Say some on synthetic images, sensitivities, calibration ans synthetic spectra.

3. Implementation

3.1. 3-dimensional imaging

The 3D setup of RLOS emulates that of its ancestor classical imaging code ([24, 25, 26]). From each pixel of the "imaging" side, of the 3D computational domain (Figure 1), a line of sight (LOS) is drawn, through the imaged volume. Along the LOS, the equation of radiative transfer is solved at each cell, using local emission and absorption coefficients. Depending on the situation modelled, coefficients may either be calculated directly, or outsourced to another program.

Lines of sight are drawn, starting from a pixel of the yz-side or xz-side (either way called the imaging side) of the domain, tracing their way along the given direction (Figures 1 and 2), until they reach a length of $\sqrt{(x_{max}^2 + y_{max}^2 + z_{max}^2)}$, where $x_{max}, y_{max}, z_{max}$ are the dimensions, in cells, of the computational domain. In practice, on reaching the ends of the domain a LOS calculation halts, therefore some LOS's end up shorter than others. The above process is repeated within a 2D loop, running over the imaging plane, each LOS corresponding to a
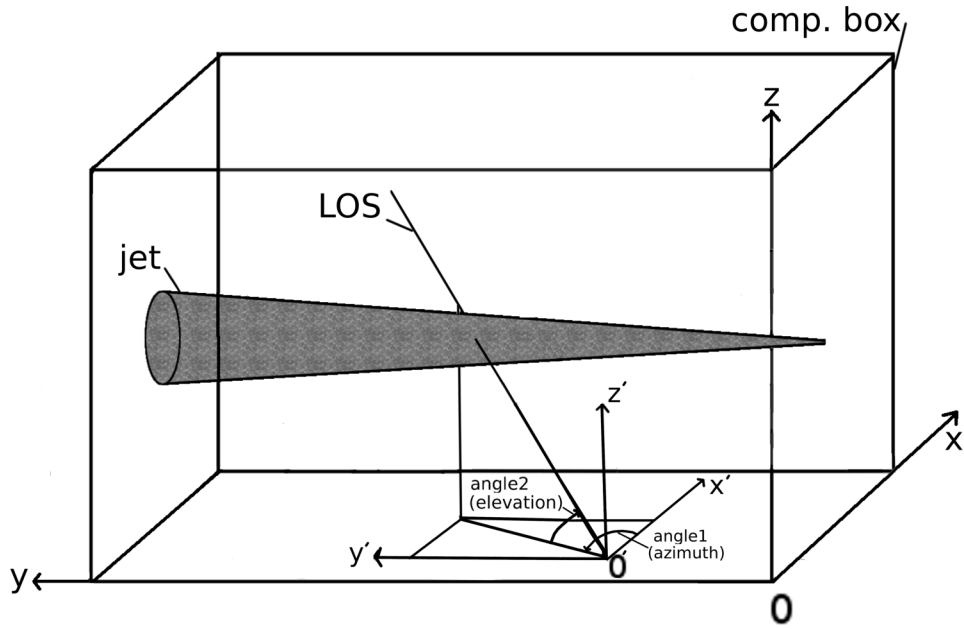
5

Figure 1: A 3D schematic view, of RLOS applied to a model astrophysical jet. The imaging side of the computational box is the yz plane, located on the side of the box apparently closer to the reader. Lying on the yz plane, O′ is the point of origin of a random LOS, with its own dashed coordinate system x′y′z′. Alternatively, the imaging plane may also lie on the xz side of the box. The final image is formed on the eye or detector of a fiducial observer, situated at the end of the LOS, through parallel transport.

single pixel of the final synthetic image. Along a LOS, no sideways scattering is considered SOS 290319 DIG UP REF for that cos ref2 asked why no scsttering? SOS.

A model astrophysical system may be inserted into RLOS directly, for example forming a 'conical' jet setup [27]. Alternatively, data output from a hydrocode may be employed, which is the case in the current paper, using PLUTO [28].

3.2. Time-resolved imaging

3.2.1. Accessing 4-dimensional data

The finite nature of the speed of light affects the appearance of a fast-moving object in a crucial manner. Consequently, drawing a relativistic image of an astrophysical system, necessitates the availability of information regarding not only its spatial properties, but its temporal evolution as well. In our case, when executing the hydrocode, before running RLOS, we adjust the temporal density of snapshots, to be saved to disk at regular intervals. The smaller those intervals, the better the temporal resolution of hydrocode data. A series of snapshots shall then be loaded to RAM by RLOS, which therefore requires a multiple quantity of memory, in order to run properly, than the hydrocode itself. Time is measured in simulation time units, which are read by PLUTO's attached 'pload.pro' routine, which loads data into RLOS.

The total time span available to a LOS, $\Delta t_{LOS(total)} = t_{(last-shot)} - t_{(first-shot)}$ [1] (as measured in simulation time units, *not* merely in number of snapshots), should be preset to be larger than the light crossing time of the model system, at the selected LOS angle settings. Documenting the model jet evolution generally requires hydrocode data saves to be rather dense in time, especially for fast-changing flows. On the other hand, a lower temporal resolution will probably suffice for a steadier, slower-paced flow.

3.2.2. Traversing the 4D arrays

Introduction. A series of hydrocode snapshots are loaded to RAM, populating the elements of 4-dimensional (4D) arrays. From a *temporal* point of view, we begin from the simulation time corresponding to the first of the loaded snapshots, called shotmin. From a *spatial* point of view, we start at the first point of the imaging plane, which is a side of the computational box (Figure 1). As the calculation advances, in 3D space, along the LOS being drawn (Figure 2), the algorithm keeps checking whether to jump to a new *temporal* slice, while

---

[1]Not to be confused with the interval Δt_{shot} between *successive* snapshots
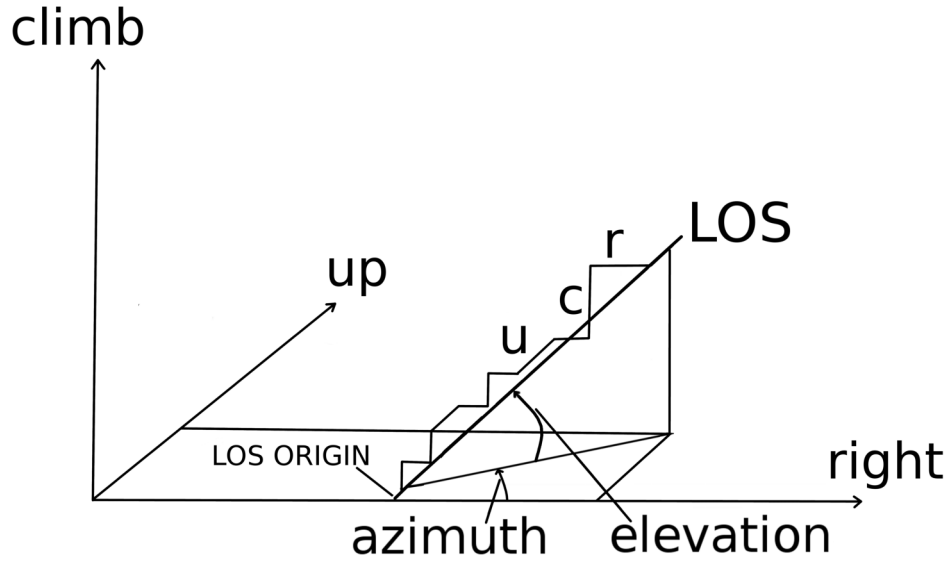
7

Figure 2: A schematic of the spatial propagation of the line of sight (LOS) through the 3D Cartesian computational grid. In the discrete grid, according to the design of the algorithm, there are 3 available directions to be taken at each step along the LOS: *right*, *up* and *climb*. These correspond to x, y and z, respectively. During propagation, the LOS 'tries' to follow its given direction, as defined by the two angles of azimuth and elevation. More specifically, every two steps a decision if first made on azimuth, either right or up. Then, for elevation, it is either climb, or another azimuth decision. In the Figure, along the LOS, horizontal steps point to the 'right' direction. Diagonal steps represent going 'up', while vertical ones constitute 'climb' steps.

staying 'on target' in 3D (Figure 3). Consequently, the LOS advances in time, through data (Figure 4), by accessing succesive instants from the 4D data arrays.

Time-resolved imaging calculations. For every LOS, there is a point of origin (POO), located on the "imaging side" of the computational grid (Figure 1). That point, addressed in the code as (nx10, ny10, nz10) and here as O′, is the beginning of the LOS's axes x′, y′, z′, parallel to x, y, z respectively. A 2D loop covers the imaging surface, the POO successively locating itself at each of the latter's points.
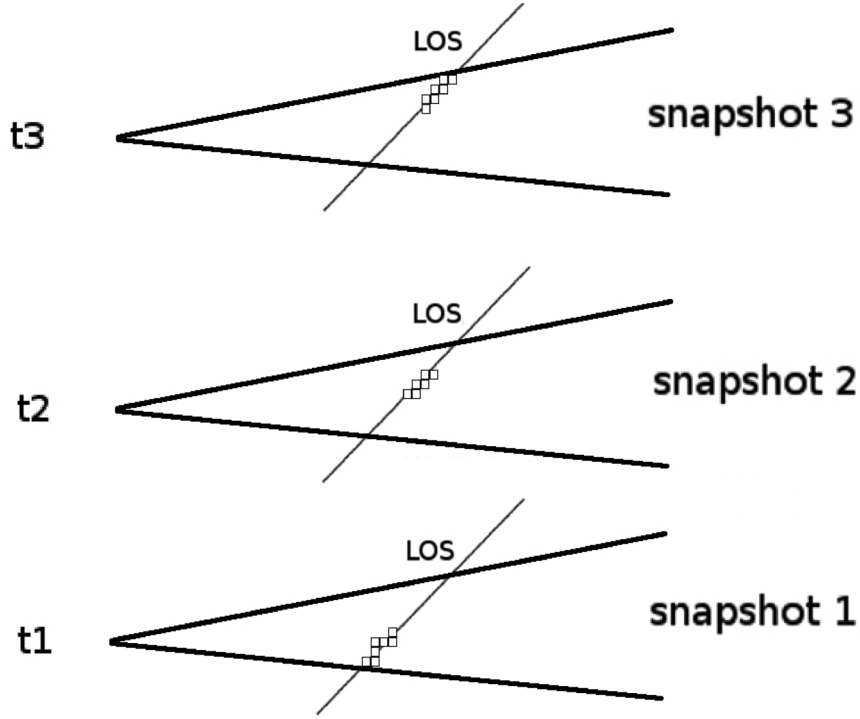
8

Figure 3: Three successive instants of a line of sight traversing a jet. At regular intervals, we jump to a new 3D slice of a 4D spacetime array, obtaining a discrete approximation of the time continuum, in the form of hydrocode snapshots.

As we progress along a LOS, a record is kept of where we are, in 3D space. This record comprises the LOS's own integer coordinates, rc, uc, and cc, measured, in cells, from its POO. The above symbols stand for right-current, up-current and climb-current, representing the current LOS advance in the x', y' and z' axes, respectively (Figures 1 and 2). The current ray position is then (nx10+rc, ny10+uc, nz10+cc).

A timer variable, curtime (standing for current LOS time), is introduced for each LOS, recording the duration of insofar ray travel along the LOS. The aforementioned timer is preset at the beginning of each LOS, to the hydrocode time of the first loaded data snapshot.

We then proceed to calculate the current length of the LOS

$$l_{los(current)} = [(dlr * (nx1current - nx10))^2 +$$
$$(dlu * (ny1current - ny10))^2 + (dlc * (nz1current - nz10))^2]^{1/2} \qquad (1)$$

9

where the LOS length is measured in cell length units and

$$nx1current = nx10 + rc, \ ny1current = ny10 + uc, \ nz1current = nz10 + cc \quad (2)$$

Along the x, y and z directions, dlc, dlu, dlr are the respective *normalized* hydrocode cartesian cell lengths. Their values are usually unity, or close to unity, as set in the hydrocode by the user, and RLOS requires them fixed, meaning only homogeneous grids are currently supported. Furthermore, if the hydrocode grid is read, by pload, at a reduced resolution, then RLOS cell sizes are automatically adjusted accordingly.

We can finally write

$$l_{los(current)} = [((dlr * rc)^2) + ((dlu * uc)^2) + ((dlc * cc)^2)]^{1/2} \quad (3)$$

We then proceed to calculate curtime, the current hydro simulation time of the light ray along the LOS.

$$curtime = l_{los(current)}/c_{light} + t_{0(LOS)}. \quad (4)$$

$t_{0(LOS)}$ is the timestamp of the first loaded snapshot, when the LOS begins to be drawn, from its point of origin, and clight is the speed of light, in cells per simulation second.

When curtime exceeds the next snapshot's timetag, the algorithm switches to drawing the LOS through the 3D volume of the next available snapshot (Figure 3). We keep moving along the same LOS in 3-D space, but we have just shifted to a new instant in the time records of the hydrocode. The above temporal shift is repeated as many times as required by the relevant criterion along the LOS, until the spatial end of the LOS.

3.2.3. Aiming the line of sight

The direction of a LOS in 3D space is defined by the two angles of azimuth (angle 1) and elevation (angle 2) (Figure 1), where the plane of angle 1 is the x'y' plane, parallel to xy. For a jet parallel to the y axis, the angle between the local jet matter velocity $\vec{u}$, and the LOS, losu=$(\widehat{\vec{LOS}, \vec{u}})$, is usually small, when

10

angle 1 approaches 90 degrees, and vice versa (Figure 5). As is well known [11], the angle losu affects the relativistic emission calculations.

Short of jet precession occuring, the plane of angle 2 (elevation) is largely perpendicular to the jet when angle 1 is zero, while it is roughly parallel to the jet when angle 1 is 90 degrees. Usually, the jet bears an approximate cylindrical symmetry, meaning that for a small angle 1, by varying angle 2, we 'rotate' the view around the jet axis, producing similar intensities throughout the way. In summary, for a jet moving along the y axis, the smaller angle 1 is, the less difference varying angle 2 makes.

On the other hand, for angle 1 nearing $\pi/2$, varying angle 2 rotates the view within a plane approximately parallel to the jet, resulting to considerable differences. Consequently, the larger angle 1 is, the stronger the effect, on the synthetic image, from changing angle 2.

3.3. Relativistic Effects

The main effects of the Lorentz/Poincaré transform on the emission from a relativistic object [6], specifically applied to an astrophysical jet, are relativistic aberration, time dilation and frequency shift [10, 11, 29, 30].

3.3.1. Lorentz factor

The Lorentz factor for a hydrocode cell is [11]

$$\Gamma_{Lorentz} = \frac{1}{\sqrt{1 - u^2}} \tag{5}$$

where

$$u = \sqrt{u_x^2 + u_y^2 + u_z^2} \leq 1 \tag{6}$$

is the value of the local velocity $\vec{u} = (u_x, u_y, u_z)$, in units of the speed of light.

3.3.2. Doppler factor calculation

Jet radiation is either boosted or de-boosted, depending on the angle losu, between the direction of the LOS and $\vec{u}$. The higher the jet speed, the narrower and stronger the cell boost cones around the jet head direction. On the other
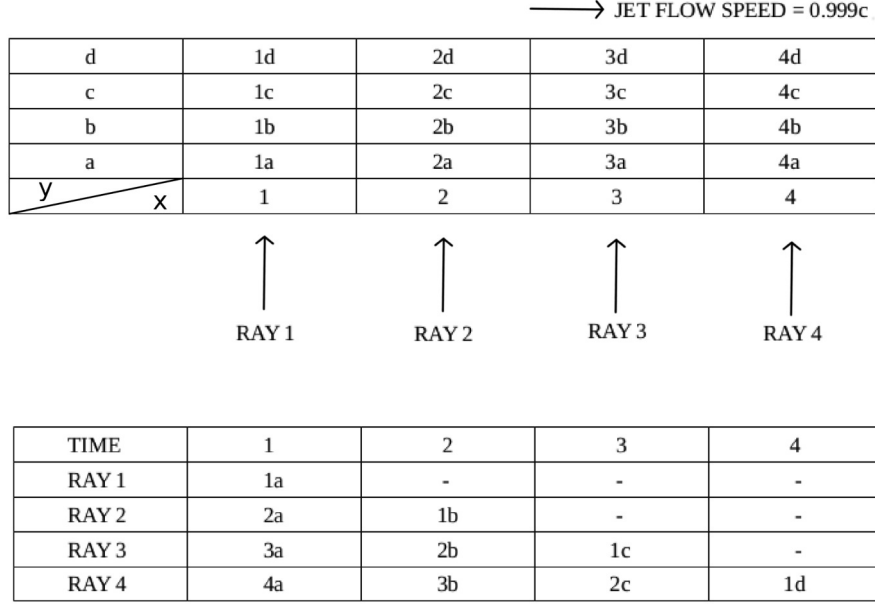
JET FLOW SPEED = 0.999c

d	1d	2d	3d	4d
c	1c	2c	3c	4c
b	1b	2b	3b	4b
a	1a	2a	3a	4a
y x	1	2	3	4

RAY 1   RAY 2   RAY 3   RAY 4

TIME	1	2	3	4
RAY 1	1a	-	-	-
RAY 2	2a	1b	-	-
RAY 3	3a	2b	1c	-
RAY 4	4a	3b	2c	1d

Figure 4: Simultaneous advance, in both space (2D) and time, of a few lines of sight. Top half depicts the spatial situation at t=1. Sixteen jet matter portions currently occupy this mini 4 by 4 grid. Each piece of matter is named after its position at t=1 and retains that name as it moves along. The bottom half shows how the situation evolves as time marches on, with light rays meeting different jet segments that cross their path. A dash means a light ray meeting jet matter other than the above, or nothing at all.

hand, outside cell boost cones, *de*-boosting occurs, that is to say the higher the velocity is, the weaker the signal becomes. D equals

$$D = \frac{\sqrt{1 - u^2}}{(1 - u * cos(losu))} \tag{7}$$

The cosine of angle losu is calculated in the following manner:

Let us define a fiducial unitary LOS vector $(\vec{LOS}) = (lx_1, lx_2, lx_3)$, with $(LOS) = \sqrt{lx_1^2 + lx_2^2 + lx_3^2} = 1$. In the following, ϕ_1 and ϕ_2 represent known angles 1 and 2, respectively.

$$lx_1 = cos(\phi_1)cos(\phi_2), \ lx_2 = sin(\phi_1)cos(\phi_2), \ lx_3 = sin(\phi_2) \tag{8}$$

$$\vec{LOS} * \vec{u} = (LOS) * u * cos(\widehat{\vec{LOS}, \vec{u}}) \tag{9}$$

12

$$LO\vec{S} * \vec{u} = lx_1 * u_x + lx_2 * u_y + lx_3 * u_z \tag{10}$$

Therefore, from equations 9 and 10, we have

$$cos(\widehat{LO\vec{S}, \vec{u}}) = \frac{lx_1 * u_x + lx_2 * u_y + lx_3 * u_z}{(LOS) * u} \tag{11}$$

Since (LOS)=1, and from equations 6 and 11, we obtain

$$cos(\widehat{LO\vec{S}, \vec{u}}) = \frac{lx_1 * u_x + lx_2 * u_y + lx_3 * u_z}{\sqrt{(u_x^2 + u_y^2 + u_z^2)}} \tag{12}$$

A miniscule number is added to the denominator of equation 12, in case u=0. The above calculation allows the assignement of a Doppler boosting factor, through equations 6, 7 and 12, to each discrete emission event along a line of sight.

3.3.3. Doppler boosting

The jet spectrum is given by

$$S_{jet} = SOS - JET - FRAME - SPECTRUM - PUT - HERE \tag{13}$$

Earth frame jet emissivity S_{obs} can be expressed [11, 10] as (SOS REF2 says Sjet is spectrum, Dtothe3plusa is emissivity)

$$S_{obs} = S_{jet}D^{3+\alpha} \tag{14}$$

where α is the spectral index. The exponent $(3+\alpha)$ in the above can be broken down into different contributions from separate effects. Two units come from the aberration of light, one from the relativistic dilation of time and α from the effect of frequency shift, while for a continuous optically thin jet a D factor is lost [10] SOS BRIEFLY EXPLAIN THIS FROM CAWTHORNE IN HUGHES 1991 SOS DO IT.

Power-law frequency shift. Radiation emitted at a given frequency, from fast-moving jet matter, is taken to be Doppler shifted in frequency
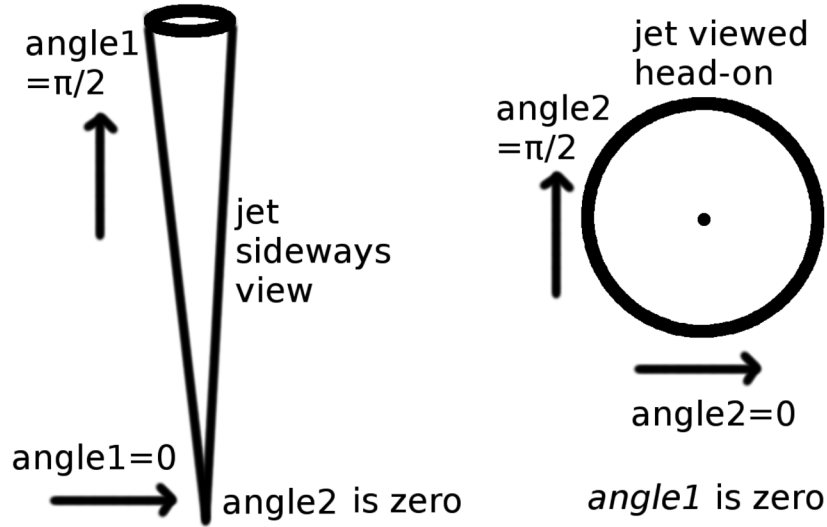
$$f_{obs} = f_{calc}D \tag{15}$$

13

Figure 5: The geometric arrangement with regard to the viewing angles in the model, for the special cases of angle2 = 0 (left) and angle1 = 0 (right). For each sub-case, the arrow shows the direction of the LOS, which is different than the reader's direction of view.

where f_{obs} is the observed frequency and f_{calc} is the frequency used in the emission calculations, performed in the jet frame of reference [11]. In order to accomodate for the shift, a power-law spectrum, falling off with frequency, is employed

$$S_{obs(f)} \propto f^{-\alpha} \tag{16}$$

with α assumed, as an approximation, to take the value of $\alpha = 2.0$, generally referring to the optically thin region of the jet. For D ≥ 1, emission is calculated at a frequency lower than the observed, resulting to a higher intensity, since the spectrum employed generally decreases with frequency.

Alternative frequency shift. RLOS may include different emission dependencies on frequency, where we calculate intensity at f$_{calc}$ and observe that at f$_{obs}$.

SUPER SOS 290319 ref2 here and generally clarify OBS vs JET. Also, consider Cawthorne's 1991 page 199 simple syncrotron jet model. as a concrete example for a user spectrum SOS.

14

At the moment, the above is included only as a quantitative indicator, where intensity may be optionally multiplied by the square of the ratio $f_{calc}/f_{obs} = 1/D^2$, partially negating the effect of Doppler boosting.

Aberration-searchlight effect. Relativistic aberration changes the perceived direction of light, when transforming between the jet frame and the earth frame, 'tilting rays', emanating from the jet, towards its head area. A jet element is assumed, for simplicity, to emit isotropically in its own frame of reference (see Cawthorne 1991, for a relevant discussion). Consequently, two Doppler factors representing aberration, are employed. SOS BASED ON HUGHES 1991, JUSTIFY the two DB factors of aberration. We multiply the intensity of each emission event, by the event's own D^2. For reasons of efficiency, this takes place for each cell, for each snapshot, before the main loop. Cell emission along a ray *within* the cell's boost cone, is then reinforced accordingly, while if *outside* the cone it is weakened. Depending on the local velocity value and direction, succesive or neighbouring cells may have totally different boost cones.

put existing tests in the appendix and [perhaps add an application to a real system.

Time dilation. Time dilation contributes one D factor to the emission result.

4. Application to a real astronomical system (keep everything short!)

SOS FROM HERE TO END PUT ALL STUFF TO THE APPENDIX, apart from the conclusions SOS.

SOS thereis no curving in SR.

WE can further on examine a focused visualization ray tracing approach. but that is a further work to be done. BEAR in mind though that our current method is like an xray, so it does not provide depth sense. so we may miss the apparent rotation effect for example. It should be straightforward though to do a focued version, since from the ficus fiducial point behind the screen we draw LOS's, each one with its own angles, from each screen point to the focal point.

15

Should be easy to implement within existing code, as an option. And it should give us more realistic images. Also, important to consider reflection, color, etc. ray tracing stuff. But NOT now! not for this paper!

5. RLOS210

141119 We now have finished RLOS version 2.10. It includes a unified, functionalized, modular approach. Both XZ and YZ versions have now been unified, for both focused beam amd also parallel LOS's. Latest tests as suggested at the start of this paper draft! Also, we add some description to this paper fo the new version. Code completely re-written now!

subsectionRLOS210 commentary transcript

****

****

131119 RLOS 2.10 code description.

Make this also into a new section in the rlos paper.

This is the latest version of rlos. Version 2 is a major upgrade of the original rlos code. This time the program is broken up into procedures and functions, with a modular structure.

The program allows the user to select which case to simulate, through an external parameter file rlos_params_v245.txt. There is a unified approach, where the same modules operate on different geometries, through parameterization.

The user may select the values of the parameters of rlos version 1, and fully employ them. As menitoned above, there is no more a different version of rlos for XZ and YZ plane image formation. Now, there is one version of the code for both cases. Furthermore, for each of those cases the user may select either radiograph or camera obscura imaging tachnique.

Radiograph has all Lines of Sight parallel to each other, just like rlos v.1. This means the film (fiducial imaging screen) is the size of the scene (grid), like an X-ray medical image. The latter type of image shows clearly the various details of the system.

16

On the other hand, camera obscura, or focused beam, has a focal point, where the eye of the fiducial observer is located. The imaging screen, in camera obscura, is also of varied size: It may be equal, or smaller to the grid slice, at a given point along either x or y axis, depending on YZ or XZ imaging plane case. At the moment, the fiducial imaging screen must be parallel to the corresponding side of the grid, i.e. either XZ or YZ. Screen location on-axis may vary within the grid. The smaller the screen, the smaller the image.

The focal point may reside either on the side of the grid, or outside the grid, BUT within the limits of the projection of the XZ or YZ plane. It may have negative or zero axis position, but its two planar coords must be smaller than the grid size.

Directino angles are no longer necessarily constant throughout the calculation: for the focused beam case, each LOS is drawn with a different set of azimuth (phi1) and elevation (phi2) angles. Angles are calculated using the lines that connect the focal point and the imaging screen point, which is the target point for the LOS.

The LOS then begins from the focal point, if it resides on the grid side, or from the LOS entry point, calced suitably (here recent relevant calc, upgrade of bversion 2.10). From then on, it advances using aiming algos, trying to pass through the targeted screen point. It normally gets the target, or misses it closely! In general, the higher the resolution, the better the accuracy in this respect.

SOS for GR pseudo-Newtonian sim, logical next step is to introduce D(phi1), D(phi2), i.e. alter angles aALONG a LOS, from cell to cell, according to the effect of the potential.

Then, jet production may be imaged, if the hydrocode can employ external forces from a Kerr BHole.

SOS ADD A FIGURE HERE in the rlos paper version of this text.

17

5.0.1. Back in time integration along the LOS

In this version, calculations may be done either ahead in time, or backwards in time, from a selected time instant (tpicked) backwards. For camera obscura, back in time is generally the correct way to proceed. For radiograph, ahead in time also works fine, assuming a suitable fiducial setup of the jet system vs the observer. tpicked is only employed when back in time switch is activated in the external param file. tpicked must be generally towards the end of the pre-selected range of dump files, or timeshots, to be loaded to RAM. Suffcient backwards time range must be provided, for the LOS to travel back through time without reaching the beginning of the gris. Else, code cannot finish integration along LOS. When testing, the facility of altering light speed, from rlos1, may be used to play and study this effect.

Pathfinding algos have been upgraded for this version. For each combination of XZ or YZ and radiograph or camera obscura, a certain set of such pathfinders are employed.

141119 figures do: a 3D-geometry figure (inclding the screen, the focal point, the focused beam, the old one is radiograph, this one shall be fbeam, also XZ vs YZ basics do include in this fig), a back-in-time figure, a block diagram of the functions SOS important.

SOS also do a figure for rlos2.10 externalparams like a table not figure

ADD THE FIGURES INTO THE PAPER OF RLOS1 but do a new section and a new version of the paper. From that paper, draw and do the 3-4 pgs new paper.

TBContinued

****

****

171119 tpicked is a param read from external param file! CAREFUL HERE! clarify we now set tpicked to t(shotmax)! We hare NOT USING tpicked any moar! SOS! $tpicked_f un = t_f un(shotmax_f un)$

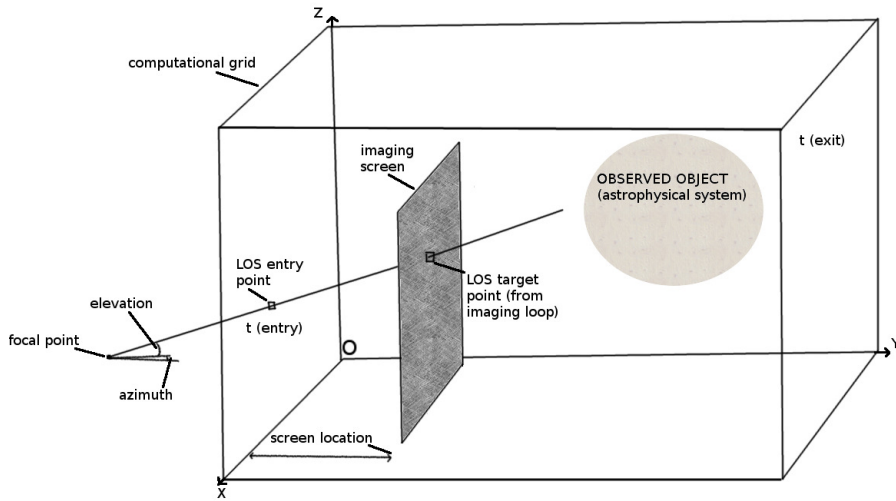161119 SOS erased, circa line 5000, the re-opening of param file!

Figure 6: First and only part of the first batch of the results.

****

NEMISS comment, also applies here indorectly!

071119 it works!!! we have the following: lxi's: the same x and z between rlos and nemiss. vi's: OPPOSITE (x of rlos is z of nemiss and vice-versa) phi1,phi2 the same from rlos to nemiss aaaaafun: OPPOSITE z and z among rlos and nemiss cccccfun:the same SO we did a 'reverse' function for aaaaa and there we reversed vx and vz. We then also created a cososureverse which finally MATCHED rlos's one!

Do tidy up here and make it nice

SOS after some points here, uanl gives ZERO! WTF? CHECK it out, esp. vs above loops! What vould it be?

040419 FROM HERE TO END ALL INTO APPENDIX PUT SOS

5.1. The rlos_param_v245.txt external parameter file

datapath (filesystem location of both hydro data and rlos)

'Our path appears here.'

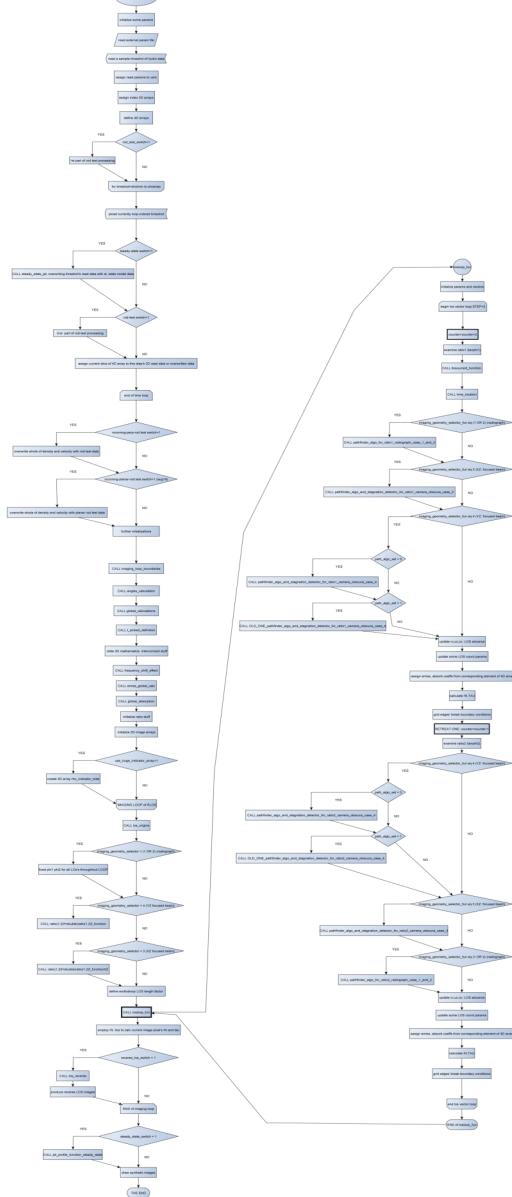*conditional_stop* (0=NO, 1=YES: use stops along the execution line)

19

Figure 7: A flow diagram of rlos2.1, depicting the procedures and functions called during program execution. A separate sub-diagram is provided for the main subroutine that draws the LOS.

0

debug_comments (0=NO, 1=YES: show debug interim results during execution)

0.0

sfactor_external (pload's shrink factor)

2.0

speedtweakfactor_external (ts speadtweak factor)

1.0

clight_override_external (0=NO, 1=YES: override clight using clight preset

20

380 value)

1.0

clight_preset_external (clight override factor)

1.2

jet_norm_velocity_external

385 0.8

shotmin_external

3

shotmax_external

97

390 *phi2_external* no D at end for mathematica usage we cut it!

0.005

phi1_external

0.005

freqshiftchoice_external

395 1.0

dopplerchoice_external

1.0

alphaindex_external

2.0

400 *nobs_external*

8000000000.0

NLONG_external

150.0

plutolength_external

405 10000000000

plutospeed_external

30000000000

plutodensity_external

0.0000000000000000000000167

410 *plutocelllength_external*

10000000000

LOOP_LENGTH_FACTOR_FOR_TIMING_RELATED_TESTS=text_array(44)/1.0D next factor reduces overall LOS length, back in time as it progresses, in order to allow for smaller time spans to be used. LOSES FAR END OF DOMAIN THOUGH, only for studiyng near effects, such as the perp. beam test!

0.930

show_loops_switch=text_array(46)/1.0D 250419 show_loops_switch is a switch that turns on ONLY showing the loop indices. It works best when rest of comments are turned OFF, else it is LOST in the clutter, thus rendered useless.

1.0

show_loops_switch__screen_boundaries=text_array(48)/1.0D another switch to omit detail here if needed

0.0

zigzag_factor=text_array(50)/1.0D zigzagfactor multiplies endlosloop which is the diagonal length of the domain. 210419 reason is that due to zig zag, even though length is e.g. 70, counter reaches 120. And zig zag affects counter, not length! This wan not set up correctly back then! Still, it was progress. 210419 HEAVILY affects execution time! MOVE TO RLOSPARAMS TXT FILE! 210419 optimal value is where it barely reaches end of domain now it is at 1.4,, else LOS ends prematurely. If it reaches ends of domain, it BREAKS anyway.

1.4

focused_beam_switch=text_array(52)/1.0D 180419 ALTERED IN imaging_loop_boundaries, according to imaging geometry selector (selected geometry)! Switch turns on focused beam. Else we should eventually get the radiograph, with parallel los's. Under construction!

0.0

focal_point_x=text_array(54)/1.0D focal point's x coordinate, zero for now! but may become neg? to allow for imaging whole grid!

-300.0

slice_x_axis_percentage=text_array(56)/1.0D SOS this is x axis percentage of

22

slice x coord.

0.80

slice_y_lower_percentage=text_array(58)/1.0D

0.15

slice_z_lower_percentage=text_array(60)/1.0D

0.15

slice_y_upper_percentage=text_array(62)/1.0D

0.15

slice_z_upper_percentage=text_array(64)/1.0D

0.15

pload_float_factor=text_array(66)/1.0D SELECTS FLOAT INSTEAD OF DOUBLE Binary DATA

1.0

ERROR_STAGNANT_LOS=0.0 next we zero the detector of stagnant los events along a los! affects

0.0

rho_indicator_Value is painting LOs voxels with a value, within a 3D indicator array

10000000000

use_huge_indicator_array=text_array(72)/1.0D this delares a huge indocator array for all LOSes!

0.0

focal_point_y_axis_percentage axis portion where fpoint is located along y

0.500

focal_point_z_axis_percentage axis portion where fpoint is located along z

0.500

imaging_geometry_selector (**SUPER SOS**) takes values 1 to 4, 1 is radiograph_xz_fun, 2 is radiograph_yz_fun, 3 is camera_obscura_xz_fun, 4 is camera_obscura_yz_fun

2

steady_state_switch SELECTS THE STEADY STATE = ON AND employs the DENSITY of the cone-like model instead of the hydrocode density. Can be either 1 (on) or zero (off)

475 0.0

rod_test_switch, SELECTS THE rod test = ON AND employs the DENSITY of the cone-like model instead of the hydrocode density.

0.0

incoming_perpendicular_rod_test_switch selects incoming perpendicular_rod_test,

480 aka relativistic test of approaching rod, wider at centre, thinner at edges 230519

0.0

incoming_planar_rod_test_switch, ruler thingy do august 2019, DO NOT SET BOTH TO ONE SOS MAKE IT FOOL PROOF SOON ENOUGH!!! SOS!!! 150519

485 0.0

halfwidth: halflength of rod 300319

2

characteristic_value_unique: unique value to set rod values equal to, in order to select them afterwards if equals that! 300319

490 1.768657846578D

ujet_steady_state: here define a steady-state jet velocity along y, the jet axis. no other velocity component is present is case the steady-state is ON. 200319

0.9

lossolidangle is the los solid angle, see code for details where it is used! Meant

495 for radiograph version, must check for cam_obsc! 150619

0.000001

LOOP_LENGTH_FACTOR_FOR_TIMING_RELATED_TESTS factor reduces overall LOS length, back in time as it progresses, in order to allow for smaller time spans to be used. LOSES FAR END OF DOMAIN THOUGH, only for

500 studiyng near effects, such as the perp. beam test! 080519

0.730

24

backwards_in_time SOS crucial parameter, when on (1) it draws the LOS back in time, from time t_picked. Currently, we have tpicked=t(shotmax), but it could be also set earlier if needed.. Else, fward, from t(shotmin) SOS set to 1.0, not zero!

0.0

focal_pointXZ_y (=text_array(100)/1.0D) imag case 3 sets this to ONE INST OF ZERO if zero,allows moar los to start! y location along y axis of focal point for XZ version. Zero for now! but may become neg? to allow for imaging whole grid!

-30.0

sliceXZ_y_axis_percentage This is the percentage of the y axis length where the XZ version's imaging screen (slice) is located.

0.20

focal_pointXZ_x_axis_percentage x-axis portion where fpointXZ is located along x

0.5

focal_pointXZ_z_axis_percentage z-axis portion where fpointXZ is located along z

0.5

sliceXZ_x_lower_percentage

0.15

sliceXZ_z_lower_percentage

0.15

sliceXZ_x_upper_percentage

0.15

sliceXZ_z_upper_percentage

0.15

path_algo_set which pathfinder algo set to employ (0 is the default case, 1 is the old ones for case4, moar may follow!)

0

reverse_los_switch activates reverse calc along a LOS, switable to use when absorption and backwards in time co-exist in a simulation (i.e. cam obsc and absorption, imaging cases 3 or 4 with absorption)

0

spectrum_direct_switch this turns on the use of the spectral formula, IF FS IS ON. 0 is IMPLIED SPECTRUM, 1 is s propto nu$\hat{(}$-alphaindex), 2 is left for future 'case selection' use, etc

0.0

kappa_spectr

1.0

kappa_spectr2 16 zeros default value. A constant used in the 108 direct spectrum SOS remember to check how many Dfactors should be in the direct spectra implementation

10000000000000000.0

debug_spectra_switch This allows, through the creation of additional emiss_4d arrays, to debug images based on different spectral implementations.

1.0

5.2. Testing parameters

Certain parameters, that facilitate testing RLOS, are presented here.

5.2.1. The clight parameter

Let us consider a 4D array, comprising a succession of hydrocode snapshots. The LOS traversing those data, moves at a speed of clight cells per time unit. When we artificially adjust clight to a lower value [31, 23], then the algorithm jumps to a new snapshot after spatially advancing through fewer cells. A slower LOS advances farther in time while crossing a given distance through the jet, allowing for a detailed study of the time-jumping algorithm. On the other hand, setting clight to a very high value leads to a single shot image, as we never advance to a further temporal slice.

In the current work, hydrocode runs employ the following scaling

$$L_{sim} = 10^{10} cm, \ u_{sim} = 3 \cdot 10^{10} \frac{cm}{s}, \rho_{sim} = 1.67 \cdot 10^{-24} \frac{g}{cm^3} \ t_{sim} = \frac{L_{sim}}{u_{sim}} = \frac{1}{3} s$$

$$B_{sim} = \sqrt{4\pi \rho_{sim} u_{sim}^2} = \sqrt{4\pi \cdot 1.67 \cdot 10^{-24} \cdot 9 \cdot 10^{20}} \simeq 0.137 G.$$

(17)

where t_{sim} is the hydrocode time unit, u_{sim} is the speed of light and L_{sim} is the hydrocode length unit. The cell length in the simulations is conveniently setup to the value of one model length unit $l_{cell} = L_{sim}$, leading to an intrinsic clight value of 1, verifying clight as the speed of light in cells/s. When preparing the hydrocode run, the time span, in simulation seconds, between data snapshots, should optimally be set, to $l_{LOS}/(n*clight)$. l is the LOS length, in *cells* and n is the desired number of snapshots to cover the imaged timespan. If we employ the parameter sfactor, pload's shrink factor, imaging voxels are enlarged and the calculated value of clight shrinks accordingly (sfactor regrids the hydrodata to a coarser grid). Overall accuracy then suffers somewhat, and shrinking the grid should be used only as a preview.

The value of clight may be manually overriden within RLOS, yet altering clight only affects the light ray speed, not the speed of matter. Consequently, overriding clight does not affect the relativistic emission calculations (like tweak-speed does, Section 5.2.4). An altered clight is merely an artifice, introduced in post processing, in order to explore the effect of using more, or less, temporal slices in the final image.

SOS to be continued from here 290319 SOS from draft with notes

5.2.2. The FS switch

After the hydrodata are loaded, a global operation calculates, for each cell, a jet frame frequency f_{calc}, from the common observing one f_{obs}: $f_{calc} = f_{obs}/D$. The frequency shift (FS) switch selects between using the local f_{calc} or the global f_{obs} in the emission calculations. In this paper, a boost of D^α)(SOS clarify obs vs jet spectrum ref.2 comment 2 par. 3) already simulates an *implied* dependence on frequency. The FS facility allows for a direct user-defined

x- loop (loops over 2D side of comp. box.)

y-loop

1D loop along the LOS
For each point on the side of comp. box, a LOS is drawn, starting there

Pathfinding algo draws 1D LOS through 3D spatial volume.
LOS timer keeps track of when to jump to a **new temporal slice**.
Then, keep going spatially, till the end of grid.
At end of LOS, assign intensity to the xy point of origin=> synthetic image formed.

ENDLOOP=> I(LOS), τ(LOS), t(LOS)
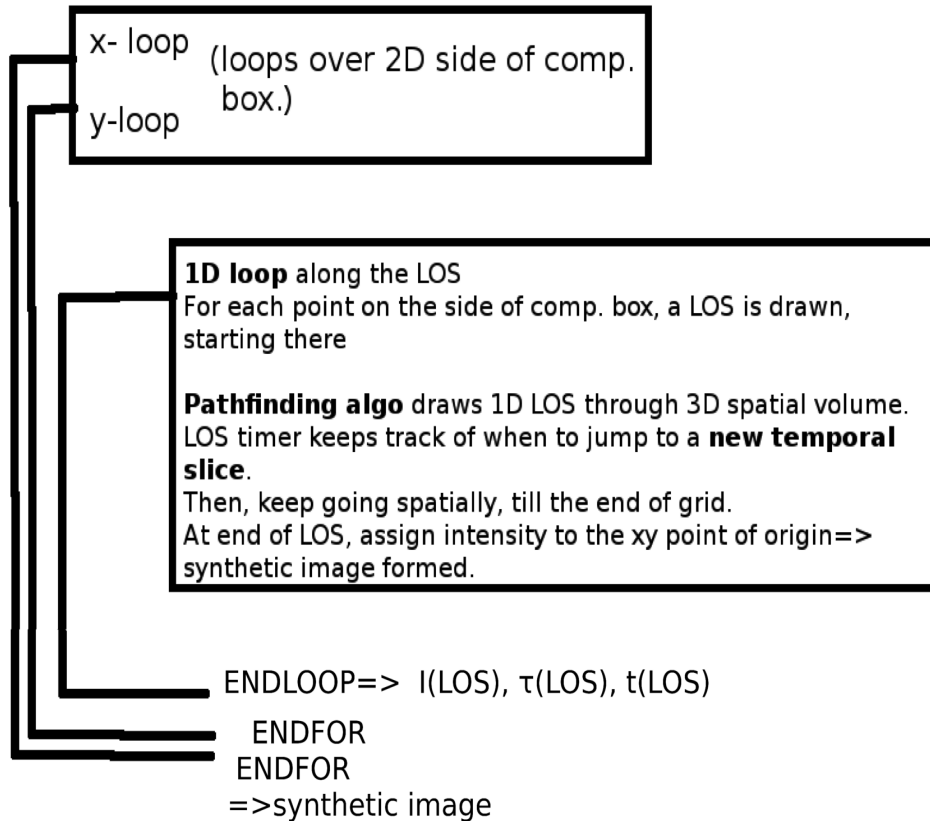
ENDFOR
ENDFOR
=>synthetic image

Figure 8: A simplified flow diagram depicting the basic logical structure of RLOS imaging code. The synthetic image's xy loops here correspond to either the yz or the xz side plane of the computational box.

emission dependence on frequency to be introduced (Cawthorne 91 pg. 199 Simplified synchrotron jet.), in the form of of a function $S_{obs} = S_{obs()f)}$, such as $S_{obs=SOSHERESYNCFORMULAHJ88}$ from synchotron emission ([27]). As an approximation, emission in the jet frame is taken to be isotropic (ref SOS hughes et al.book isotropic in jet frame, e.g. for sync OK due to tangled B field. Anyhow, this is ok for 1st approximation).

5.2.3. The DB switch

The DB switch offers the option of using the Doppler boosting effect, in the form of $D^{3+\alpha}$.

28

A test is introduced, where matter velocity is multiplied, on a global scale, by a 'speed tweak' factor. This offers a quick way to observe the impact, on the synthetic image, of altering the hydrodynamic speed in post-processing, for the same simulation run. The natural value of tweakspeed is 1. At low tweak speed factors (less than 1) the effects, on the final image, of both DB and FS, are reduced, and vice versa. The maximum for tweakspeed is $c/u_{(max)}$, above which velocites higher than c are artificially created in the grid.

5.2.5. An example

As an example, we distinguish four different combinations of DB and FS. Emissivity is measured in arbitrary units, common for all cases.

1. Both DB and FS turned on.

$$S_{obs} \propto \rho D^{3+\alpha}(\frac{f_{calc}}{f_{obs}})^2 = \rho D^{1+\alpha} \tag{18}$$

2. DB turned on, FS turned off.

$$S_{obs} \propto \rho D^{3+\alpha} \tag{19}$$

3. DB turned off, FS turned on.

$$S_{obs} \propto \rho(\frac{f_{calc}}{f_{obs}})^2 = \frac{\rho}{D^2}, \tag{20}$$

4. DB turned off, FS turned off.

$$S_{obs} \propto \rho \tag{21}$$

6. Description of RLOS

RLOS is written for the IDL or the GDL programming languages, and is released under the LGPL licence. It replaces its classical ancestor, as part of a suite of simulation and visualization programs that study astrophysical jets, in a perceived numerical laboratory. The latter combined approach employs a hydrocode, LOS code, a visualization package, and a number of in-house gamma-ray [25, 26] and neutrino emission calculation programs [32, 33]. The addition of RLOS to the above software suite, aims to reinforce the realism

29

of the imaging part of the calculations. Finally, the modular structure of the program facilitates the inclusion of more physical effects in the future.

RLOS is organized in two outer spatial loops, running over the imaging plane and an inner 1-dimensional spatial loop, advancing in pairs of steps, one for each angle, running over the length of a LOS. At the innermost lies a *conditional* temporal loop, running over the hydro data time span. The basic structure of the algorithm can be seen in Figure 8. Since much of the calculation load is global, it is performed, where feasible, before the loops, in array-oriented operations, in order to improve performance.

6.1. Steady-state tests here

1. test vs ours mnras 2014.

2. test vs literature: e.g. KRaus (focused rlos vs kraus. Then unfocused rlos vs focused rlos.) SOS unfocused rlos SOS KEEP IT COS IT WORKS WITH PLUTO calc neutrinos as userdef var where theta is fixed all over pluto. SOS only use unfocused as a eye candy, and as comp. to obs. DO PROVE their equivalence, i.e. image from opposite sides and unfocused presumes opposite side image creatrion).

3. Synthetic images and synthetic spectra. HERE DACE emply interpolation possible with PSO to select nodes for interp.

7. Results and discussion

7.1. Model setup

SOS DO RUN TESTS USING THE NEWLY INSERTED STEADY-STATE MODEL. DEVICE A FEW TESTS FOR COMPARISON WITH KNOWN CASES.

PLUTO data clear description here.

The hydrocode data that serve as input to RLOS tests, are the result of a few simulation runs of a relativistic astrophysical jet. The hydrocode used is PLUTO, set to employ its RMHD (relativistic magneto-hydro-dynamic) module.

30

The model jet is magnetized with a toroidal component, resulting to magnetic collimation.

Data saved in dbl format include density, pressure, velocity, the 3 components of velocity (in units of c), for every computational cell and for every time node (data save). The units of the above are (units place here form existing text)

In this Section, RLOS is tested under different circumstances, based on just a few underlying hydrocode runs. This way, the effect of altering each parameter on the final synthetic image is examined.

Jet emission is first calculated in the jet frame of reference, which frame is different for each cell. Emission ois taken to be proportional to density, as a simple way to test the code. In general, emission may be expressed by a formula suitable for the EM band employed.

Radiation then travels along a LOS towards the fiducial observer. Along the LOS, the equation of radiative transfer is solved (SOS say why no-side ways scattering SOS).

HERE eqn of rad transfer. SOS

An intermittent model jet, representing a microquasar system, injected at $u_{jet} = 0.26c$, 0.6c or 0.8c is studied with the RMHD setup of the PLUTO hydrocode, at a uniform grid resolution of $60 \times 100 \times 60$. In all of the model runs the same initial jet density of 10^{10} protons/cm^3 is used, 10 times less than the maximum surrounding gas density. Winds comprise an accretion disk wind construct and a stellar wind, which falls off away from the companion star, located off-grid at (400, 0, 400), while the jet is threaded by a strong confining toroidal magnetic field of B=400 simulation units. Blobs are emitted during the first 1.5 out of every 10 time units (simulation seconds), for both the u=0.26c and the u=0.8c models, while for the u=0.6c case, the jet is on during the first 5 out of every 50 time units. The simulations were run until at least t = 750, saving a data snapshot every 15 time units. Taken from the u=0.6c model run, a snapshot of density is shown in Figure 9, in both 2D and 3D, where we can see the magnetically collimated sequence of plasmoids advancing through

31
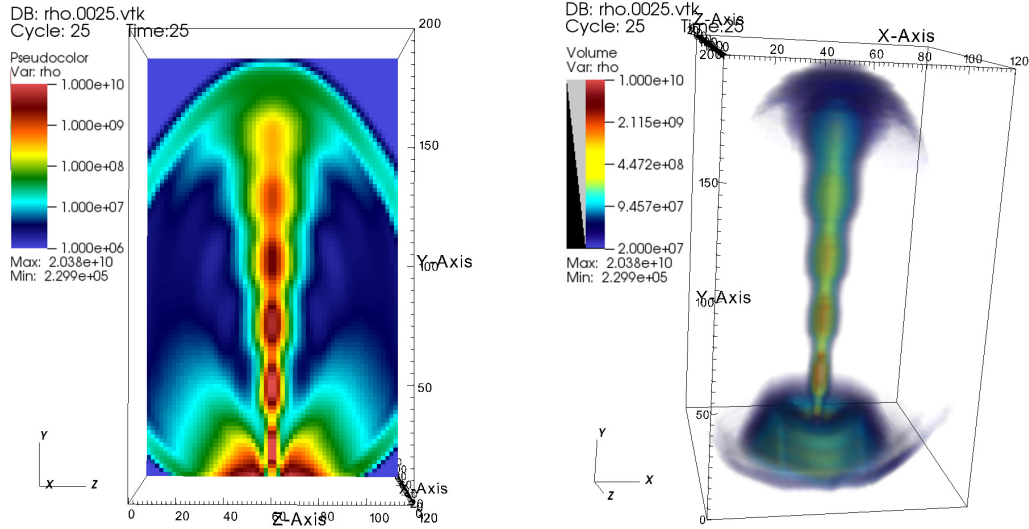
Figure 9: Snapshot 25 of the u=0.6c hydrocode run, corresponding to a model time of t=375 (25 × 15), depicting the density. We can see the jet front reaching the end of the grid, having advanced though increasingly lighter surrounding winds, after crossing the simplified accretion disk wind construct. On the left is presented a slice cut throught the data and on the right a 3-dimensional density plot. Image produced with VisIt.

surrounding winds.

RLOS was then run, based on the above hydrocode data, with sfactor=1 for the pload shrink factor. In general, the imaging process may or may not use all snapshots available to it, depending on the light crossing time of its model segment (potentially adjusted through the clight parameter). Trying to read more snapshots than loaded corrupts the hydrocode time array, called T, resulting to errors.

The synthetic images are *logarithmic* plots of intensity. Emissivity is proportional to matter density, using the same arbitrary scale everywhere. Doppler boosted intensity is proportional to D^{3+a}, for an optically thin jet comprising a series of plasmoids [10]. No self absorption is employed, even though the feature is available for future use.

Later on in this Section, comparisons between different runs of the imaging code are presented, demonstrating the effect of altering a given parameter, on
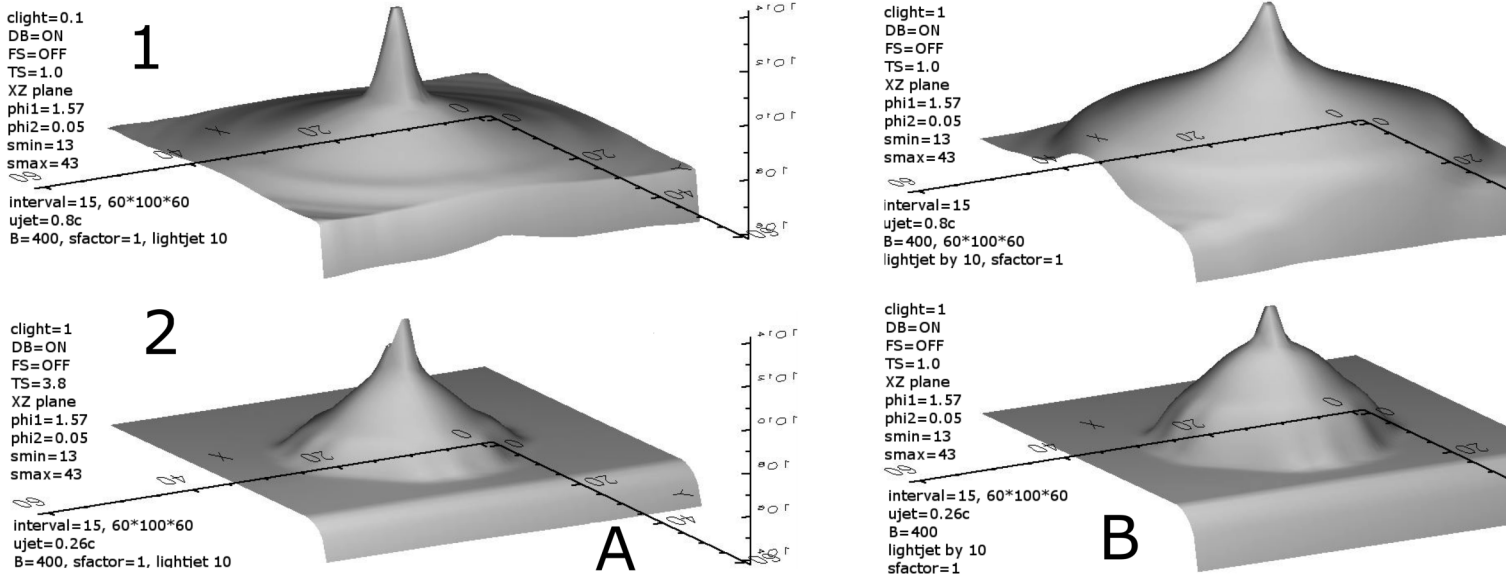
32

clight=0.1
DB=ON
FS=OFF
TS=1.0
XZ plane
phi1=1.57
phi2=0.05
smin=13
smax=43

interval=15, 60*100*60
ujet=0.8c
B=400, sfactor=1, lightjet 10

1

clight=1
DB=ON
FS=OFF
TS=1.0
XZ plane
phi1=1.57
phi2=0.05
smin=13
smax=43

interval=15
ujet=0.8c
B=400, 60*100*60
lightjet by 10, sfactor=1

clight=1
DB=ON
FS=OFF
TS=3.8
XZ plane
phi1=1.57
phi2=0.05
smin=13
smax=43

interval=15, 60*100*60
ujet=0.26c
B=400, sfactor=1, lightjet 10

2

clight=1
DB=ON
FS=OFF
TS=1.0
XZ plane
phi1=1.57
phi2=0.05
smin=13
smax=43

interval=15, 60*100*60
ujet=0.26c
B=400
lightjet by 10
sfactor=1

A

B

Figure 10: First and only part of the first batch of the results.

the synthetic image. Each run is identified by both its information tag and by a chessboard-like 2D pair of alpha-numerical coordinates, referring to the multi-Figures (Figures 10, 11, 12, 13, 14, 15, 16).

We now define the following correspondences: Process 1 page 1 is shown in Figure 10, process 2 page 1 in Figure 11, process 2 page 2 in Figure 12, process 2 page 3 in Figure 13, process 3 page 1 in Figure 14, process 3 page 2 in Figure 15, process 4 page 1 in Figure 16.

The synthetic images are referred to as follows: (process or 'batch' number, page or 'part' number, alphanumeric coordinate, imaging data). For example, (1, 1, 1A, data) means process 1, page 1, line 1, column A. The 'data' part contains values of certain imaging parameters, ts standing for tweakspeed, clight for itself, a1 for angle 1 and a2 for angle 2, both measured in radians, DB for
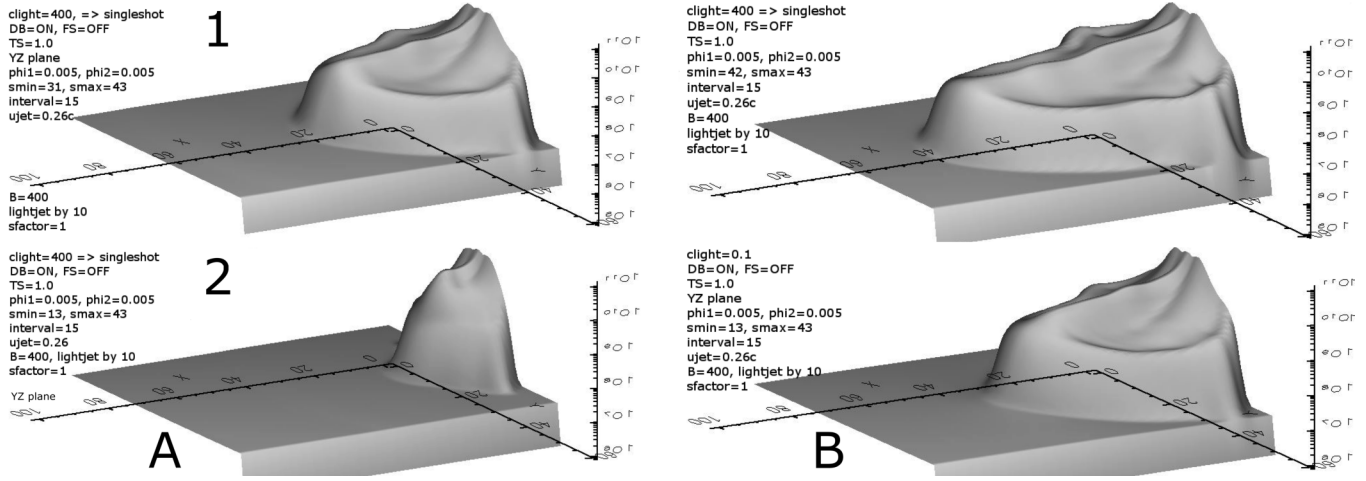
33

Figure 11: First part of the second batch of the results.

the Doppler boosting switch and FS for the frequency shift switch, smin/max
are the first and last among the snapshots employed, the imaging plane (xz or
yz), and u_{jet} is the nominal injection speed of the jet matter. In the annotated
Figures of the results, phi1 and phi2 are the two angles of azimuth and elevation
respectively, and snapshotmax is the maximum snapshot count of a LOS. Each of
the following subsections describes the effects that changing a certain parameter
has on the synthetic image.

7.2. Viewing angles

A pair. (process2, page2, 1B, ts=1.0, clight=1, a1=0.59, a2=0.005, DB=on,
FS=off, smin=37, smax=43, u_{jet}=0.26c, YZ) vs
(process2, page3, 1A, ts=1.0, clight=1, a1=0.005, a2=0.005, DB=on, FS=off,
smin=37, smax=43, u_{jet}=0.26c, YZ)

Comment: When angle 1 is small, the LOS is nearly perpendicular to the
jet, depicting the object clearly. The larger angle 1 becomes, the more off target
the image is created. If angle1 approaches $\pi/2$, the jet is observed nearly along
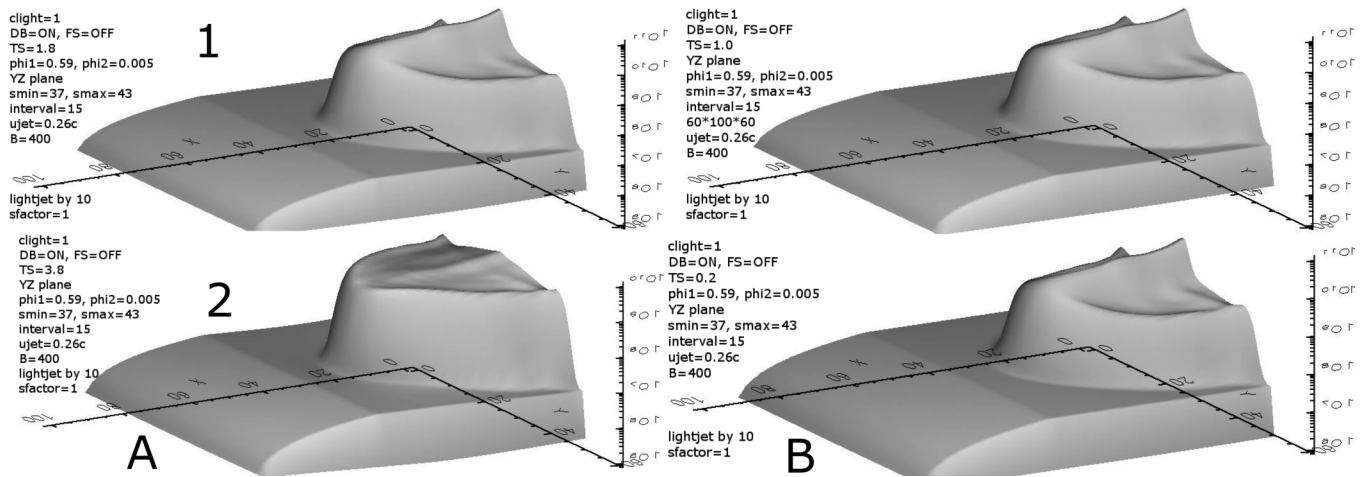its axis. Then, it is time to draw the image on the XZ imaging plane.

34

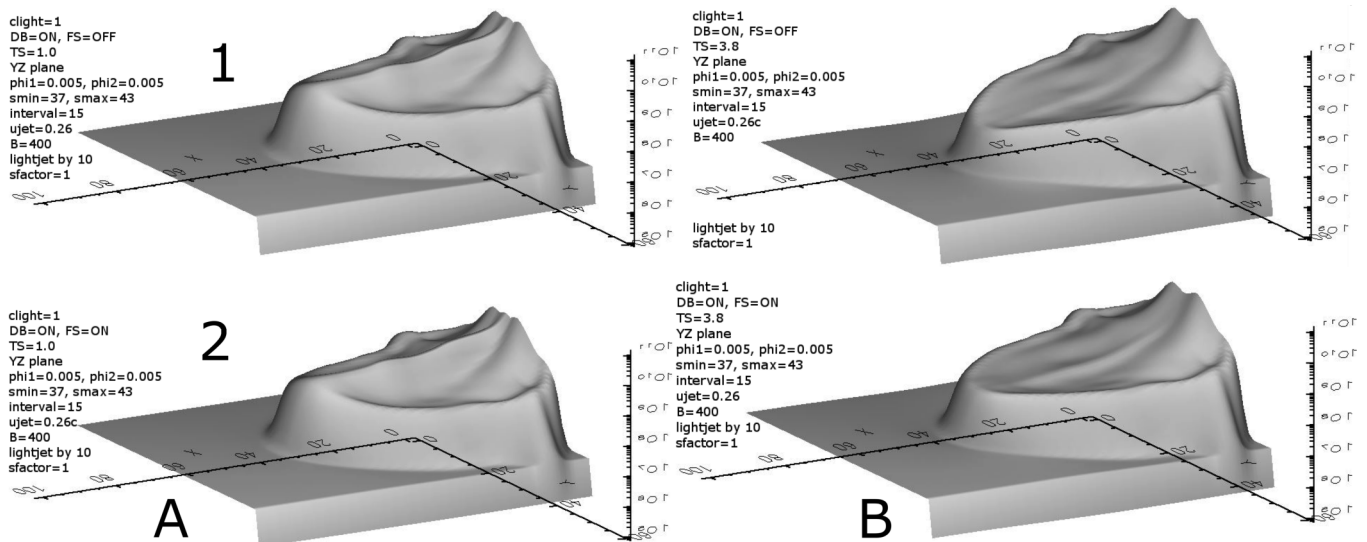Figure 12: Second part of the second batch of the results.

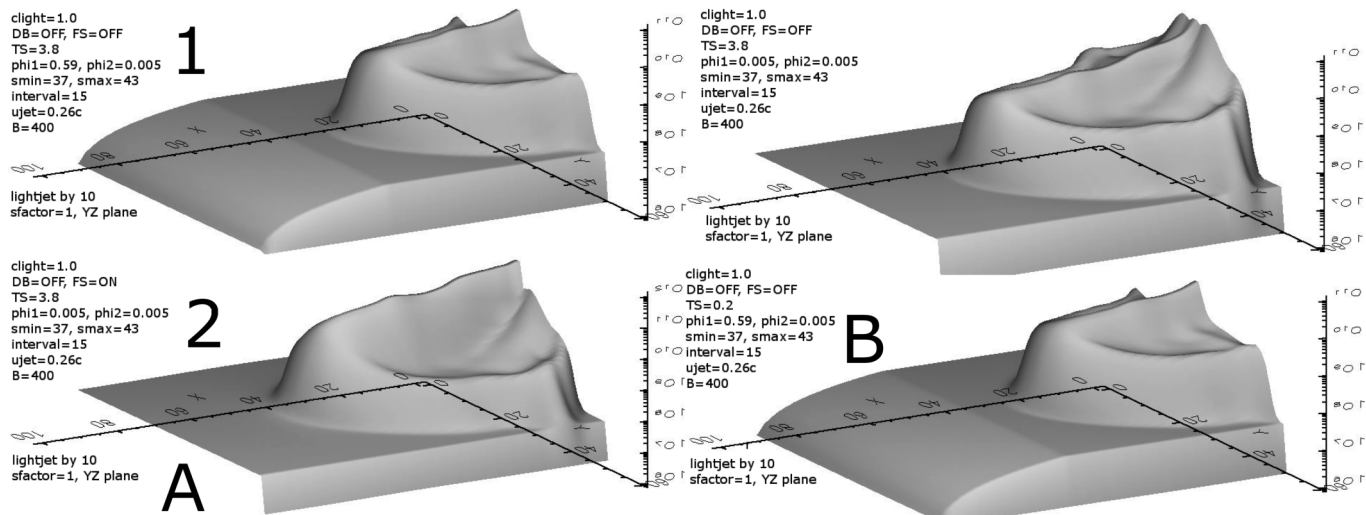Figure 13: Third part of the second batch of the results.

Figure 14: First part of the third batch of the results.

A pair. (process4, page1, 1A, ts=1.0, clight=1, a1=0.45, a2=0.005, DB=on, FS=off, smin=18, smax=23, u$_{jet}$=0.6c, YZ) vs

(process4, page1, 2A, ts=1.0, clight=1, a1=0.45, a2=0.35, DB=on, FS=off, smin=18, smax=23, u$_{jet}$=0.6c, YZ)

Comment: Angle 2 is varied here, at a large angle 1. Consequently, the view is rotated, within the plane of elevation, around a direction non-parallel to the jet, resulting to quite large differences between the two images (Section 3.2.3).

A pair. (process4, page1, 1B, ts=1.0, clight=1, a1=0.005, a2=0.35, DB=on, FS=off, smin=18, smax=23, u$_{jet}$=0.6c, YZ) vs

(process4, page1, 2B, ts=1.0, clight=1, a1=0.005, a2=0.005, DB=on, FS=off, smin=18, smax=23, u$_{jet}$=0.6c, YZ)

Comment: Angle 2 is varied here, this time at a *small* angle 1. As a result, the view is rotated around a direction nearly parallel to the jet, resulting to much smaller differences between the two images, as compared to the previous pair.

36

clight=0.1
DB=OFF
FS=OFF
TS=1.0
XZ plane
phi1=1.57
phi2=0.05
smin=13
smax=43
interval=15, 60*100*60
ujet=0.8c
B=400, sfactor=1, lightjet 10

1

clight=1
DB=OFF
FS=ON
TS=1.0
XZ plane
phi1=1.57
phi2=0.05
smin=13
smax=43
interval=15
ujet=0.8c
B=400, 60*100*60
lightjet by 10, sfactor=1

clight=1
DB=OFF
FS=OFF
TS=3.8
XZ plane
phi1=1.57
phi2=0.05
smin=13
smax=43
interval=15, 60*100*60
ujet=0.26c
B=400, sfactor=1, lightjet 10

2

A

clight=1
DB=OFF
FS=OFF
TS=1.0
XZ plane
phi1=1.57
phi2=0.05
smin=13
smax=43
interval=15, 60*100*60
ujet=0.26c
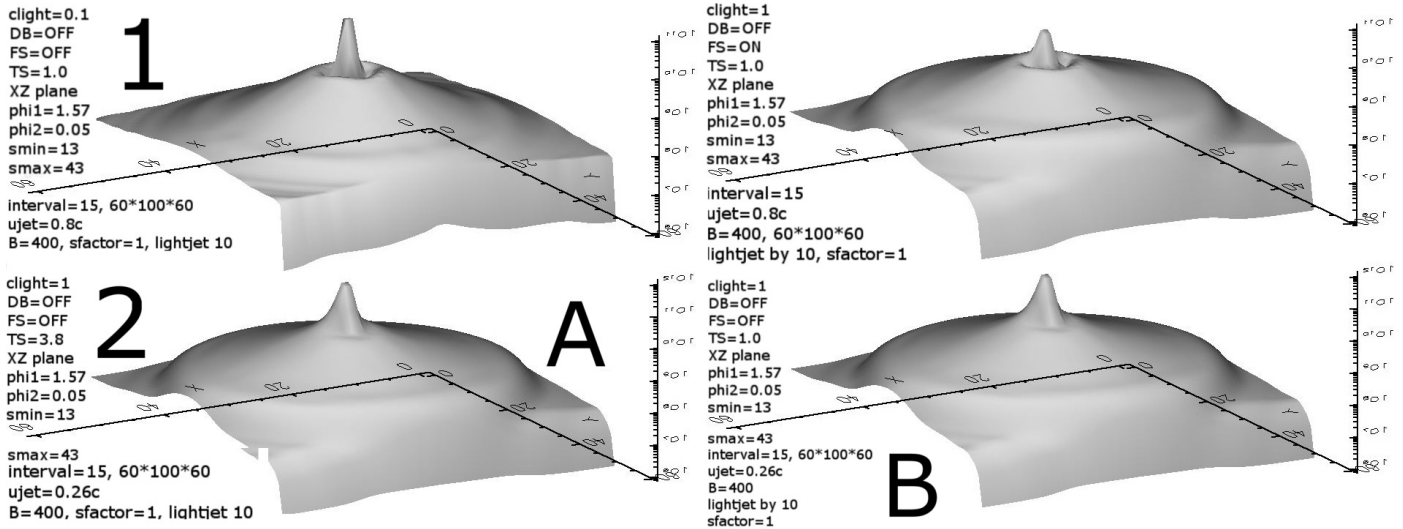**B=400**
lightjet by 10
sfactor=1

B

Figure 15: Second part of the third batch of the results.

7.3. Frequency shift

A pair. (process2, page3, 1A, clight=1, ts=1.0, a1=0.005, a2=0.005, DB=yes, FS=no, smin=37, smax=43, u_{jet}=0.26c, YZ) vs

(process2, page3, 2A, clight=1, ts=1.0, a1=0.005, a2=0.005, DB=yes, FS=yes, smin=37, smax=43, u_{jet}=0.26c, YZ)

Comment: The images look almost the same, with tiny differences found along the jet axis. At such a low jet speed, the $1/D^2$ effect of FS is limited, resulting to a couple of very similar images.

A pair. (process2, page3, 1B, clight=1, ts=3.8, a1=0.005, a2=0.005, DB=yes, FS=no, smin=37, smax=43, u_{jet}=0.26c, YZ) vs

(process2, page3, 2B, clight=1, ts=3.8, a1=0.005, a2=0.005, DB=yes, FS=yes, smin=37, smax=43, u_{jet}=0.26c, YZ)

Comment: The two images look the same, except along the jet axis. There, the intensity is slightly raised when FS in switched on. At such low angles, the average losu is almost $\pi/2$, clearly outside the boost cones of most jet axis cells. Combined with such a high effective jet speed (ts=3.8), the resulting
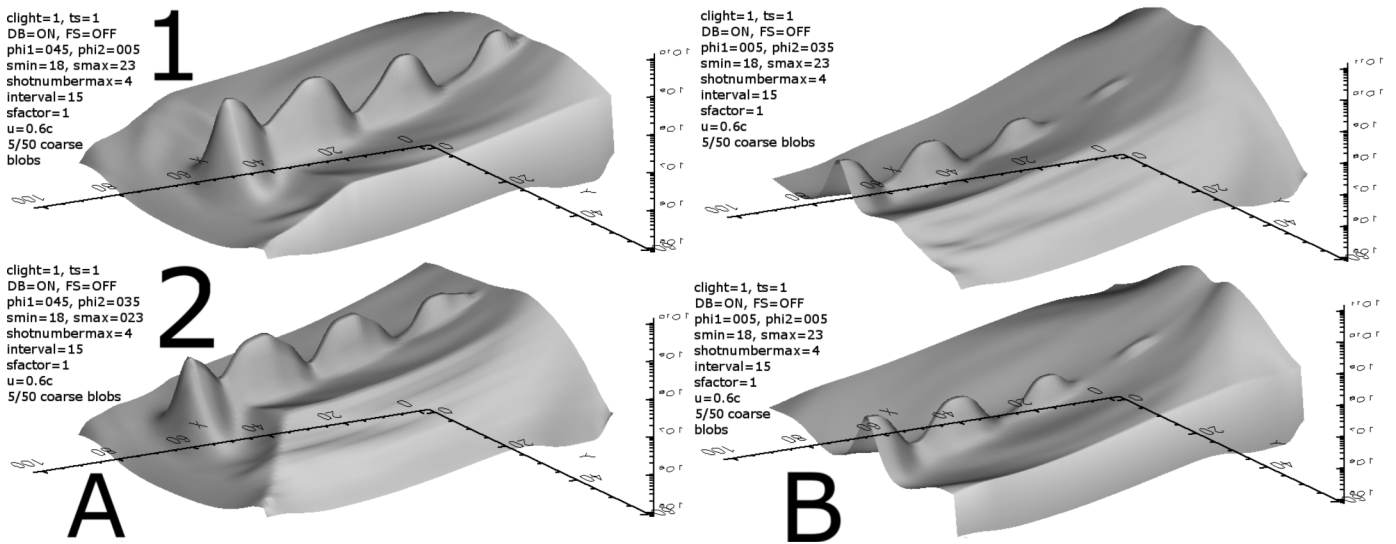
37

Figure 16: Fourth batch of the results.

Doppler factor D is quite smaller than 1. Consequently, 'losing' two D factors when FS is turned *on* (Section 5.2.5, case 2 vs case 1) leads to a detectable *increase* in emission along the jet axis. Elsewhere, velocities are lower and the differentiating effect of FS is much weaker.

7.4. Doppler boosting

A pair. (process2, page2, 2A, clight=1, ts=3.8, YZ, smin=37, smax=43, u_{jet}=0.26c, a1=059, a2=0.005, DB=yes, FS=no) vs

(process3, page1, 1A, clight=1, ts=3.8, YZ, smin=37, smax=43, u_{jet}=0.26c, a1=059, a2=0.005, DB=no, FS=no)

Comment: The two images in this pair are quite similar, apart from the jet axis region. On-axis, at such a high effective maximum velocity (ts × c ≃ 0.988), most boost cones are narrow, therefore the angle 1 value of 0.59 rad places the LOS outside them, de-boosting the jet when DB is turned on. Consequently, intensity in this pair is actually higher without DB.

A pair. (process2, page2, 2B, clight=1, ts=0.2, YZ, smin=37, smax=43, u_{jet}=0.26c, a1=0.59, a2=0.005, DB=yes, FS=no) vs

38

765 (process3, page1, 2B, clight=1, ts=0.2, YZ, smin=37, smax=43, u_{jet}=0.26c, a1=0.59, a2=0.005, DB=no, FS=no)

Comment: These images look very similar, since at such a low ts factor, the effective maximum velocity is 0.26c × 0.2 = 0.052c, leading to very little relativistic boosting or de-boosting, despite the far from zero value of angle 1.

770 *A pair.* (process2, page3, 1B, clight=1, ts=3.8, YZ, smin=37, smax=43, u_{jet}=0.26c, a1=0.005, a2=0.005, DB=no, FS=no) vs

(process3, page1, 1B, clight=1, ts=3.8, YZ, smin=37, smax=43, u_{jet}=0.26c, a1=005, a2=0.005, DB=no, FS=no)

Comment: Both angles have near zero values, therefore the Doppler-boosted
775 image is much weaker (de-boosting) along the jet axis, at a maximum effective jet speed of ts × 0.26c = 0.988c. To the sides, intensities differ much less, due to low intrinsic velocities there. The above are attributed to boost cones being narrow enough to exclude from themselves this pair's LOS direction.

A pair. (process1, page1, 1A, clight=0.1, ts=1.0, XZ, smin=13, smax=43,
780 u_{jet}=0.8c, a1=1.57, a2=0.05, DB=yes, FS=no) vs

(process3, page2, 1A, clight=0.1, ts=1.0, XZ, smin=13, smax=43, u_{jet}=0.8c, a1=1.57, a2=0.05, DB=no, FS=no)

Comment: Doppler boosting is quite large in (1, 1, 1A), since angle 1 approaches $\pi/2$, lying inside the boost cones of most jet axis cells, at
785 $u_{jet(injected)}$=0.8c. When DB is turned on (1, 1, 1A), the jet base footprint appears narrower, limiting the area of stronger emission to the close vicinity of the jet axis. The reason is that speed now makes a difference and only the jet axis posesses it. In contrast, deactivating DB largely cancels the above narrowing effect. Furthermore, the 'dark ring' of reduced emission, surrounding the jet
790 axis (3, 2, 1A), represents an area vacated by the winds being pushed away to the sides and is present in the fast jet model run.

These images are drawn at low clight (0.1), causing rays to advance at 1/10 of their normal speed, employing many snapshots, beginning at smin=13. A

39

narrower jet projection results, the slower LOS reaching *later* snapshots, when
winds around the jet base have been pushed away by the jet.

A pair. (process1, page1, 2A, clight=1, ts=3.8, XZ, smin=13, smax=43,
u_{jet}=0.26c, a1=1.57, a2=0.05, DB=yes, FS=no) vs
(process3, page2, 2A, clight=1, ts=3.8, XZ, smin=13, smax=43, u_{jet}=0.26c,
a1=1.57, a2=0.05, DB=no, FS=no)

Comment: A similar case appears here, at a higher ts, where, despite the
lower clight, the boosted jet looks stronger and narrower, while the de-boosted
one is wider than before. This time the effective jet speed is 0.988c, the result
of multiplying u_{jet} and ts.

A pair. (process1, page1, 2B, clight=1, ts=1.0, XZ, smin=13, smax=43,
u_{jet}=0.26c, a1=1.57, a2=0.05, DB=yes, FS=no) vs
(process3, page2, 2B, clight=1, ts=1.0, XZ, smin=13, smax=43, u_{jet}=0.26c,
a1=1.57, a2=0.05, DB=no, FS=no)

Comment: Employing DB significantly narrows the visible part of the jet
base, while making it emit somehow stronger as well. On the other hand,
turning DB off (3, 2, 2B), leads to a wider emission base for the jet, since now
only density matters to the result.

7.5. Tweak speed

In this subsection we explore the effects, on the synthetic image, of artificially
altering, on a global scale, in post-processing, the speed of matter.

A pair. (process1, page1, 2A, clight=1, ts=3.8, XZ, smin=13, smax=43,
u_{jet}=0.26c, a1=1.57, a2=0.05, DB=yes, FS=no) vs
(process1, page1, 2B, clight=1, ts=1.0, XZ, smin=13, smax=43, u_{jet}=0.26c,
a1=1.57, a2=0.05, DB=yes, FS=no)

Comment: Both images are Doppler boosted. At an effective speed of 0.988c,
we observe an emission increase by about one hundrend times (1, 1, 2A), relative
to the image drawn at the natural speed (1, 1, 2B). The intensity profile, moving

40

from the jet periphery radially towards its axis, is steeper, spanning 7 orders of magnitude, for the artificially faster jet, as opposed to only 5 for the normal jet.

A quartet. (process2, page2, 1A, clight=1, ts=1.8, YZ, smin=37, smax=43, u_{jet}=0.26c, a1=0.59, a2=0.005, DB=yes, FS=no) vs
(process2, page2, 1B, clight=1, ts=1.0, YZ, smin=37, smax=43, u_{jet}=0.26c, a1=0.59, a2=0.005, DB=yes, FS=no) vs
(process2, page2, 2A, clight=1, ts=3.8, YZ, smin=37, smax=43, u_{jet}=0.26c, a1=0.59, a2=0.005, DB=yes, FS=no) vs
(process2, page2, 2B, clight=1, ts=0.2, YZ, smin=37, smax=43, u_{jet}=0.26c, a1=0.59, a2=0.005, DB=yes, FS=no)

Comment: Given a value of angle 1 of 0.59 rad, Doppler boosting of $1 \leq D \leq 2$ is present along the jet axis at ts = 0.2, 1.0 and 1.8 (maximum effective jet speed of 0.052c, 0.26c and 0.468c respectively). At ts = 3.8 though (0.988c), no boosting occurs along the jet, as boost cones are now too narrow, leaving out losu angles corresponding to angle 1 of .59 rad.

A pair. (process2, page3, 1A, clight=1, ts=1.0, YZ, smin=37, smax=43, u_{jet}=0.26c, a1=0.005, a2=0.005, DB=yes, FS=no) vs
(process2, page3, 1B, clight=1, ts=3.8, YZ, smin=37, smax=43, u_{jet}=0.26c, a1=0.005, a2=0.005, DB=yes, FS=no)

Comment: At an effective speed of 0.988c (2, 3, 1B), boost cones are pretty narrow, therefore at such small angles 1 and 2 as this pair's, the jet axis appears heavily *de*-boosted. On the other hand, at an effective speed of 0.26c (2, 3, 1A) the jet axis still emits significantly, at a representative value of D(u $\simeq$ 0.26c, coslosu $\simeq$ 0) $\simeq$ 0.8.

A pair. (process2, page3, 2A, clight=1, ts=1.0, YZ, smin=37, smax=43, u_{jet}=0.26c, a1=0.005, a2=0.005, DB=yes, FS=yes) vs
(process2, page3, 2B, clight=1, ts=3.8, YZ, smin=37, smax=43, u_{jet}=0.26c, a1=0.005, a2=0.005, DB=yes, FS=yes)

₈₅₀ Comment: At high effective velocities, de-boosting occurs, essentially along the jet axis. Compared to the previous pair, Doppler effects are less intense in both images here, being proportional to $D^{1+\alpha}$, as opposed to $D^{3+\alpha}$.

A pair. (process3, page1, 1A, clight=1, ts=3.8, YZ, smin=37, smax=43, u_{jet}=0.26c, a1=0.59, a2=0.005, DB=no, FS=no) vs

₈₅₅ (process3, page1, 2B, clight=1, ts=0.2, YZ, smin=37, smax=43, u_{jet}=0.26c, a1=0.59, a2=0.005, DB=no, FS=no)

Comment: Despite a huge difference in efffective speeds, no difference occurs, since both DB and FS are turned off. The sole influence left on intensity is matter density, which is identical for both images.

₈₆₀ *A pair.* (process3, page2, 2A, clight=1, ts=3.8, XZ, smin=13, smax=43, u_{jet}=0.26c, a1=1.57, a2=0.05, DB=no, FS=no) vs

(process3, page2, 2B, clight=1, ts=1.0, XZ, smin=13, smax=43, u_{jet}=0.26c, a1=1.57, a2=0.05, DB=no, FS=no)

Comment: Both DB and FS are turned *off*, therefore no apparent difference ₈₆₅ occurs between the two images.

7.6. Clight

Varying clight only affects the LOS's rate of advance, leaving intact the relativistic calculations of Lorentz and Doppler factors.

A pair. (process1, page1, 1A, clight=0.1, ts=1.0, XZ, smin=13, smax=43, ₈₇₀ u_{jet}=0.8c, a1=1.57, a2=0.05, DB=yes, FS=no) vs

(process1, page1, 1B, clight=1.0, ts=1.0, XZ, smin=13, smax=43, u_{jet}=0.8c, a1=1.57, a2=0.05, DB=yes, FS=no)

Comment: We can see here the difference slow-light relativistic imaging (1, 1, 1A) makes, compared to simply imaging at normal light speed (1, 1, 1B). The ₈₇₅ 'slow' image, formed as a combination of a longer series of snapshots, appears natural to the eye, resembling an intermediate time instant in the jet evolution. The lower the imposed speed of light is (1, 1, 1A), the less laterally developed

the jet emission appears, as later snapshots contribute less to the image (later on, surrounding winds' density, as projected on XZ, around the jet base, tends to fade).

A quartet. (process2, page1, 2A, clight=400, ts=1.0, YZ, smin=13, smax=43, u_{jet}=0.26c, a1=0.005, a2=0.005, DB=yes, FS=no) vs

(process2, page1, 2B, clight=0.1, ts=1.0, YZ, smin=13, smax=43, u_{jet}=0.26c, a1=0.005, a2=0.005, DB=yes, FS=no) vs

(process2, page1, 1A, clight=400, ts=1.0, YZ, smin=31, smax=43, u_{jet}=0.26c, a1=0.005, a2=0.005, DB=yes, FS=no) vs

(process2, page1, 1B, clight=400, ts=1.0, YZ, smin=42, smax=43, u_{jet}=0.26c, a1=0.005, a2=0.005, DB=yes, FS=no)

Comment: The result of slowing down light, by 10 times (2, 1, 2B), is compared to three effectively single shot images (clight = 400), taken at different time instants (smin × interval = smin × 15). The jet traverses a substantial portion of the computational grid during the formation of the 'slow light' synthetic image, as compared to the earliest snapshot of this group (2, 1, 2A). (2, 1, 2B) appears quite natural to the eye, resembling an intermediate snapshot, between (2, 1, 1A) and (2, 1, 1B).

8. Conclusions

RLOS has evolved from its classical ancestor LOS code, in order to address the problem of imaging model *relativistic* astrophysical jets. Despite its theoretical simplifications, the program succeeds in providing a time-delayed synthetic image of a hydrodynamical model jet, while avoiding the complexity of a more complete approach. Applications may include a variety of dynamical astrophysical phenomena, where synthetic observations are compared to actual ones, an achieved match largely validating the initial conditions of the numerical models.

RLOS tests verify the integrity of the program and demonstrate its versatility, when imaging a model astrophysical system. We also note its ability to incorporate various emission and absorption coefficients, covering different

43

wavebands, from radio to γ-rays. What's more, the use of a hydrocode allows modelling complex dynamical systems, facilitating the study of many scenarios.

Furthermore, apart from the currently employed dependence on density, emission may also be a function of the magnetic field, local velocity, and others. An example is X-ray synchrotron radiation, which also includes a direct dependence on the frequency shift effect. Certain particle emissions may even be modelled, if suitable directional relativistic expressions are employed, transforming emission from the jet to the stationary frames of reference. The inclusion of aberration is a potential next step in the program development, along with certain gravitational corrections to the ray path.

References

[1] A. Lampa, Zeitschrift fur Physik 27 (1924) 138.

[2] J. Terrell, Phys. Rev. 116 (1959) 1041.

[3] R. Penrose, Proc. Cambridge Phil. Soc. 55 (1959) 137.

[4] V. F. Weisskopf, Phys. Today 13 (1960) 24.

[5] G. D. Scott, M. R. Viner, American Journal of Physics 33 (1965) 534.

[6] D. Weiskopf, Dissertation, Ph.D. thesis, Dissertation, der Eberhard-Karls-Universitat zu Tubingen, der Fakultat fur Physik (2001).

[7] R. J. Deissler, Am. J. Phys. 73 (2005) 663.

[8] D. Weiskopf, in: H. Hagen (Ed.), Scientific Visualization: Advanced Concepts, Dagstuhl Publishing, Leibniz Center for Informatics, Germany, 2010, p. 289302.

[9] I. F. Mirabel, L. F. Rodríguez, Ann. Rev. Astron. Astrophys37 (1999) 409.

[10] T. V. Cawthorne, in: Hughes (Ed.), Beams and Jets in Astrophysics, Cambridge University Press, 1991.

[11] P. A. Hughes, in: Hughes (Ed.), Beams and Jets in Astrophysics, Cambridge University Press, 1991.

[12] D. Weiskopf, U. Kraus, H. Ruder, ACM Trans. Graph. 18 (1999) 3.

[13] R. D. Klauber, Is detection of fitzgerald-lorentz contraction possible?, arXiv:0808.1117v1 (2008).

[14] G. B. Rybicki, A. P. Lightman, Radiative Processes in Astrophysics, Wiley-Interscience, New York, 1979.

[15] A. Jarabo, B. Masia, A. Velten, C. Barsi, R. Raskar, D. Gutierrez, Computer Graphics Forum, 34 (8) 34 (2015) 1.

[16] F. R. Hickey, Am. J. Phys. 47 (1979) 711.

[17] P. Hsiung, R. Dunn, Proceedings of Supercomputing 1989 Conference 1 (1989) 597.

[18] P. Hsiung, R. Thibadeau, M. Wu, Computer Graphics 24(2) 24 (1990) 83.

[19] U. Kraus, American Journal of Physics 68 (2000) 56.

[20] T. Muller, S. Boblest, Eur. J. Phys. 35 (2014) 06502.

[21] T. Muller, Comput. Phys. Commun. 185 (2014) 2301.

[22] A. Velten, D. Wu, A. Jarabo, B. Masia, C. Barsi, C. Joshi, E. Lawson, M. Bawendi, D. Gutierrez, R. Raskar, ACM Trans. Graph. 32 (2013) 4.

[23] Z. W. Sherin, R. Cheu, P. Tan, G. Kortemeyer, Visualizing relativity: the openrelativity project, American Journal of Physics 84 (2016) 369.

[24] T. Smponias, T. S. Kosmas, MNRAS412 (2011) 1320.

[25] T. Smponias, T. S. Kosmas, MNRAS438 (2014) 1014.

[26] O. Kosmas, T. Smponias, aHEP accepted (2018).

[27] R. M. Hjellming, K. J. Johnston, ApJ 328 (1988) 600.

[28] A. Mignone, G. Bodo, S. Massaglia, T. Matsakos, O. Tesileanu, C. Zanni, A. Ferrari, Ap. J. Supp.170 (2007) 228.

[29] W. B. Sparks, D. Fraix-Burnet, F. Macchetto, F. N. Owen, A counterjet in the elliptical galaxy m87, Nature 355 (1992) 804.

[30] R. Laing, A. H. Bridle, Relativistic models and the jet velocity field in the radio galaxy 3c 31, Monthly Notices of the Royal Astronomical Society 336 (2002) 328.

[31] G. Kortemeyer, P. Tan, S. Schirra, A slower speed of light: Developing intuition about special relativity with games fdg 2013, FDG 13 Proceedings of the International Conference on the Foundations of Digital Games. ACM New York, NY, USA 1 (2013) 400.

[32] T. Smponias, O. Kosmas, Advances in High Energy Physics 921757.

[33] T. Smponias, O. Kosmas, Advances in High Energy Physics 4962741.